B PHYSICS AND QCD AT SLD

David J. Jackson*
Rutherford Appleton Laboratory,
Chilton, Didcot, Oxfordshire OX11 0QX, England

Representing the SLD Collaboration

ABSTRACT

Analysis of B decays and QCD phenomena at the SLD experiment at the SLC e^+e^- collider is presented. The results are based on a sample of 150,000 hadronic Z^0 decays collected between 1993 and 1995 together with 250,000 hadronic Z^0 decays collected from 1996 to 1998 with an upgraded vertex detector. The large longitudinal polarization of the SLC e^- beam (average $\langle P_e \rangle \sim 73\%$) was utilized by some of the measurements. The precise CCD pixel vertex detector allows efficient and pure identification of the B decay tracks.

The topics in QCD covered here include hadron production and correlations, the flavor independence of α_s, the structure of $b\bar{b}g$ events and the measurement of the B hadron energy. The B physics presented consists of measurements of the B^+ and B^0 lifetimes, a search for charmless and measurement of double-charm B decays, and B_s^0–$\overline{B_s^0}$ mixing analyses. The excluded values of the oscillation frequency Δm_s will be discussed. The results presented are preliminary.

*This work was supported in part by the US Department of Energy and the UK Particle Physics and Astronomy Research Council.

1 Introduction

Electrons and positrons from the two-mile long Stanford Linear Accelerator are brought into head-on collision by the Stanford Linear Collider (SLC) at a centre-of-mass energy of 91.2 GeV. The SLC Large Detector (SLD) collects data from the Z^0 decays produced in such collisions. About 70% of the Z^0s decay into quark (u, d, s, c or b flavor) anti-quark pairs which in turn hadronise into final state jets of particles, hence the opportunity to perform tests of QCD. During the period 1993-1998 around 400,000 hadronic Z^0 decays were recorded.

While the Z^0 boson has been studied in detail by each of the four LEP experiments at CERN (each has recorded around 4,000,000 Z^0 events), the unique features of the SLC and SLD allow for complementary analysis. The high longitudinal polarization of the SLC e^- beam allows the selection of quark or anti-quark jets. In addition, the powerful vertex reconstruction capability of the SLD 3D CCD pixel vertex detector,[1] upgraded before the 1996 run, provides a unique opportunity to tag and study B decays.

1.1 B–Tagging

The excellent vertexing capabilities at SLD are exploited in the reconstruction of B decays in $Z^0 \to b\bar{b}$ events. The analysis begins with the selection of hadronic Z^0 events. A detailed description of the experimental procedure can be found elsewhere.[2] Topological vertex reconstruction is applied separately to the tracks in each hemisphere (defined with respect to the event thrust axis) as described in detail in Ref. 3. The vertices are reconstructed in 3D co-ordinate space by defining a vertex function $V(\mathbf{r})$ at each position $\mathbf{r}$ in terms of the track parameters such that it is large in regions of high track multiplicity. Maxima are found in $V(\mathbf{r})$ and clustered into resolved spatial regions. Tracks are associated with these regions to form a set of topological vertices. The efficiency for reconstructing at least one secondary vertex in a b hemisphere is $\sim$ 50% ($\sim$ 67%) for VXD2 (VXD3 - the upgraded vertex detector).

The mass M of the reconstructed vertex is calculated by assuming each track has the mass of a pion. The minimum transverse momentum P_T of the vertex tracks relative to the vertex axis (which is varied within the 1σ limits constraining the axis at the measured interaction point (IP) and reconstructed seed vertex) is calculated in order to determine the P_T corrected mass:

$$M_{P_T} = \sqrt{M^2 + P_T^2} + |P_T|. \quad (1)$$

This quantity is the minimum mass the decaying hadron could have in order to produce a vertex with the quantities M and P_T. The tag is applied to each event hemisphere, with the resulting M_{P_T} distribution for Monte Carlo and data events as shown in Fig. 1.

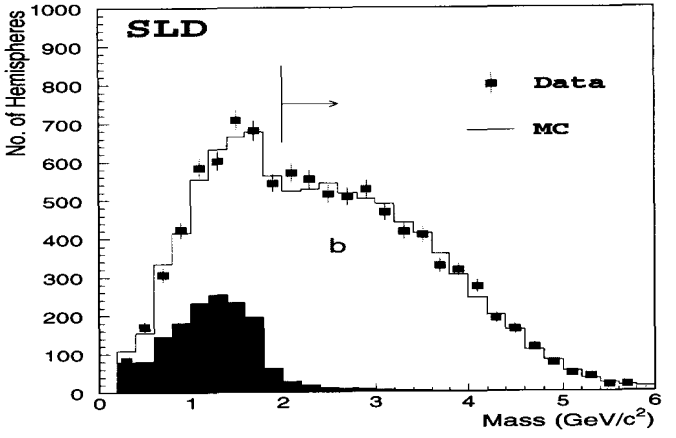

Fig. 1. The P_T corrected mass, M_{P_T}, for b (clear histogram) c (light shaded) and uds (dark shaded) Monte Carlo and data (points) events.

Requiring $M_{P_T} > 2$ GeV/c^2 (above the charm hadron mass) selects a sample of B hadrons with a purity of $\sim$ 98% and and efficiency of $\sim$ 50% using VXD3.[4] This topological vertex reconstruction is used in most of the B physics measurements as well as in some of the QCD analyses.

2 QCD

2.1 Hadron Production and Correlations[5]

The analysis in this section is based on the 1993–95 SLD data sample. The selection of tracks and hadronic events is described in Ref. 5. Samples of events enriched in light and b primary flavors were selected with a more primitive flavor

tagging technique based on signed impact parameters δ of charged tracks with respect to the IP in the plane transverse to the beam. For each event we define n_{sig} to be the number of tracks passing a set of impact-parameter quality cuts that have impact parameter greater than three times its estimated error, $\delta > 3\sigma_\delta$. Events with $n_{sig} = 0$ were assigned to the light-tagged sample and those with $n_{sig} \geq 3$ were assigned to the b-tagged sample. The remaining events were classified as a c-tagged sample. The light-, c- and b-tagged samples comprised 60.4%, 24.5% and 15.2% of the selected hadronic events, respectively.

Separate samples of hemispheres enriched in light-quark and light-antiquark jets were selected from the light-tagged event sample by exploiting the large electroweak forward-backward production asymmetry with respect to the beam direction. The event thrust axis was used to approximate the initial $q\bar{q}$ axis and was signed such that its z-component was along the electron beam direction, $\hat{t}_z > 0$. Events in the central region of the detector, where the production asymmetry is small, were removed by the requirement $|\hat{t}_z| > 0.2$, leaving 74% of the light-tagged events. The quark-tagged hemisphere in events with left- (right-)handed electron beam polarization was defined to comprise the set of tracks with positive (negative) momentum projection along the signed thrust axis. The remaining tracks in each event were defined to be in the antiquark-tagged hemisphere. For the selected event sample, the average magnitude of the polarization was 0.73. Using this value and assuming Standard Model couplings, a tree-level calculation gives a quark (antiquark) purity of 0.73 in the quark-(antiquark-)tagged sample.

2.1.1 Total Production Cross Sections

In this section we discuss details of the analysis for three categories of identified hadrons: charged tracks identified as $\pi^\pm$, $K^\pm$ or p/$\bar{\text{p}}$ in the SLD Cerenkov Ring Imaging Detector (CRID), see Fig. 2; K^0_s and $\Lambda^0/\bar{\Lambda}^0$ reconstructed in their charged decay modes and tagged by their long flight distance; and $K^{*0}/\bar{K}^{*0}$ and ϕ reconstructed in charged decay modes including one and two identified $K^\pm$, respectively.

We have integrated our differential cross sections over their respective measurement ranges, Fig. 3, taking into account the bin-to-bin correlations in the systematic errors. In order to quote total cross sections, we must extrapolate into the unmeasured regions of x_p, and we have done this using three MC models. From

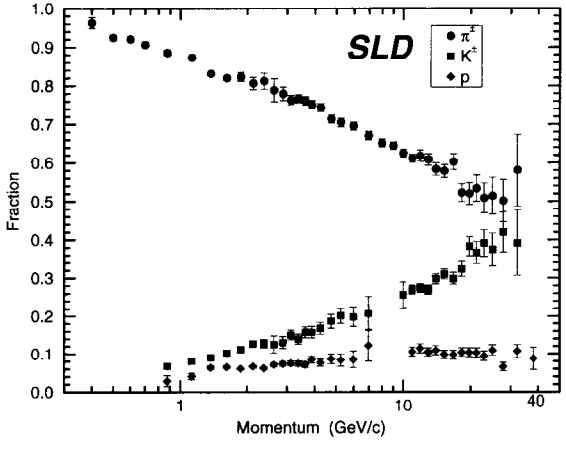

Fig. 2. Charged particle identification with the CRID.

the hadrons of each species generated using each of these models, we calculated the fraction that were generated with x_p in the range of our measurement. For each hadron species the three fractions were found to be similar, with the UCLA (HERWIG) fraction being typically 1% larger (1–2% smaller) than the JETSET fraction.

We applied the same procedure to our measurements for the three flavor categories. The three simulations were found to give similar flavor dependences, with the accepted fraction in b (c) events typically 0.02 (0.01) larger than that in light-flavor events.

2.1.2 Leading Particle Effects

We extended these studies to look for differences between particle and antiparticle production in light quark (as opposed to antiquark) jets, in order to address the question of whether e.g. a primary u-initiated jet contains more hadrons that contain a valence u-quark (e.g. π^+, K^+, p, Λ^0) than hadrons that do not (e.g. π^-, K^-, $\bar{\text{p}}$, $\bar{\Lambda}^0$). To this end we used the light quark- and antiquark-tagged hemispheres described in section 2.1.

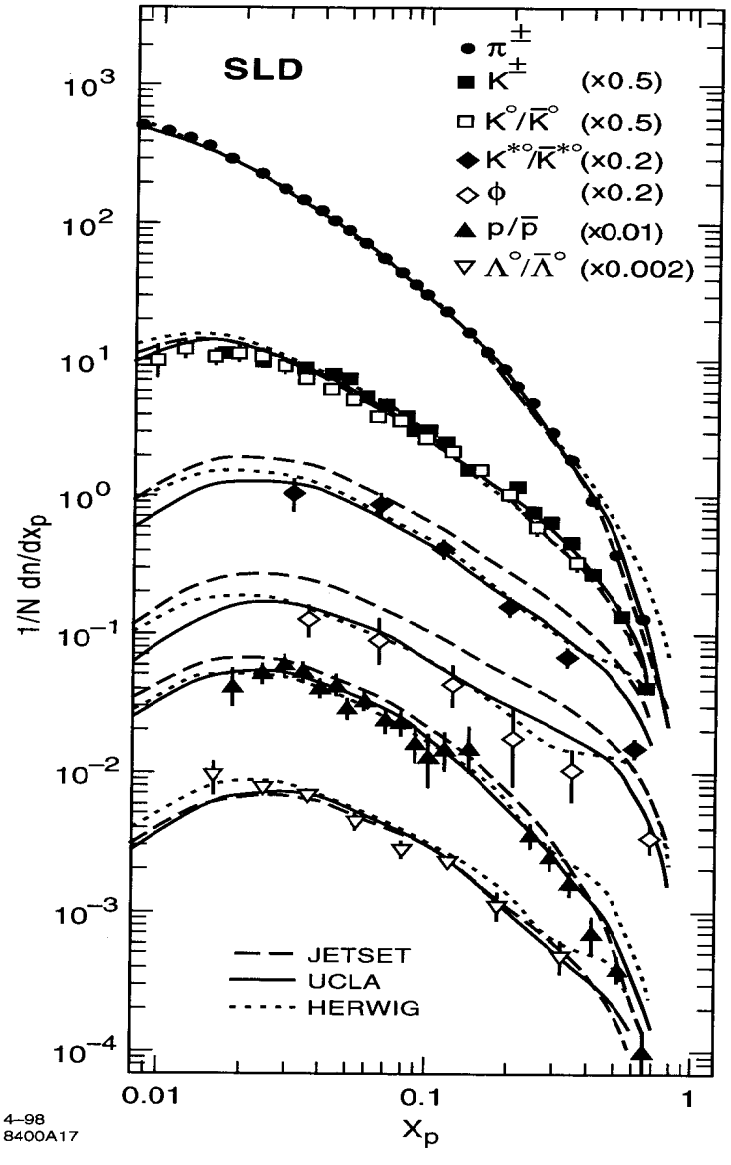

Fig. 3. Particle production in *uds* tagged events.

We measured the differential cross sections per light quark jet

$$R_h^q = \frac{1}{2N_{evts}} \frac{d}{dx_p} \left[N(q \to h) + N(\bar{q} \to \bar{h}) \right], \quad (2)$$

$$R_{\bar{h}}^q = \frac{1}{2N_{evts}} \frac{d}{dx_p} \left[N(q \to \bar{h}) + N(\bar{q} \to h) \right], \quad (3)$$

where: q and $\bar{q}$ represent light-flavor quark and antiquark jets respectively; N_{evts} is the total number of events in the sample; h represents any of the identified hadron species π^-, K^-, $\overline{K}^{*0}$, p, or Λ^0, and $\bar{h}$ indicates the corresponding antihadron. Then, for example, $N(q \to h)$ is the number of hadrons of species h in light quark jets. This formulation assumes CP symmetry, i.e. $N(q \to h) = N(\bar{q} \to \bar{h})$, which was found to be satisfied in the data in all cases.

The charged hadron fractions analysis was repeated on the sample of positively charged tracks in the quark-tagged jets and negatively charged tracks in the antiquark-tagged jets, yielding measured values of $R_{\pi^+}^q$, $R_{K^+}^q$, and R_{p}^q in the tagged samples. The same procedure applied to the remaining tracks yielded $R_{\pi^-}^q$, $R_{K^-}^q$, and $R_{\bar{\mathrm{p}}}^q$. The $K^{*0}/\bar{K}^{*0}$ and $\Lambda^0/\bar{\Lambda}^0$ analyses were applied similarly to the quark- and antiquark-tagged jets to yield $R_{\overline{K}^{*0}}^q$, $R_{K^{*0}}^q$, R_{Λ}^q and $R_{\bar{\Lambda}}^q$.

It is convenient to show the results in the form of the difference between hadron h and antihadron $\bar{h}$ production normalized by the sum:

$$D_h = \frac{R_h^q - R_{\bar{h}}^q}{R_h^q + R_{\bar{h}}^q}. \quad (4)$$

A value of zero corresponds to equal production of hadron and antihadron, whereas a value of +(−)1 corresponds to complete dominance of (anti)particle production. As shown in Fig. 4 in each case the difference is consistent with zero at low x_p. For charged pions it is also consistent with zero at high x_p, but for the other hadrons there are significant positive differences that appear to increase with increasing x_p.

The results for the baryons [Figs. 4(a) and 4(b)] afford the most straightforward interpretation. Since baryons contain valence quarks and not antiquarks, the observed excess of both protons and Λ^0s over their respective antibaryons for $x_p > 0.2$ is clear evidence for the production of leading baryons. The data suggest that the effect increases with x_p, however more data are needed to study the x_p dependence in detail. For $x_p < 0.2$ the data are consistent with equal production of baryons and antibaryons, however the contribution from fragmentation is very

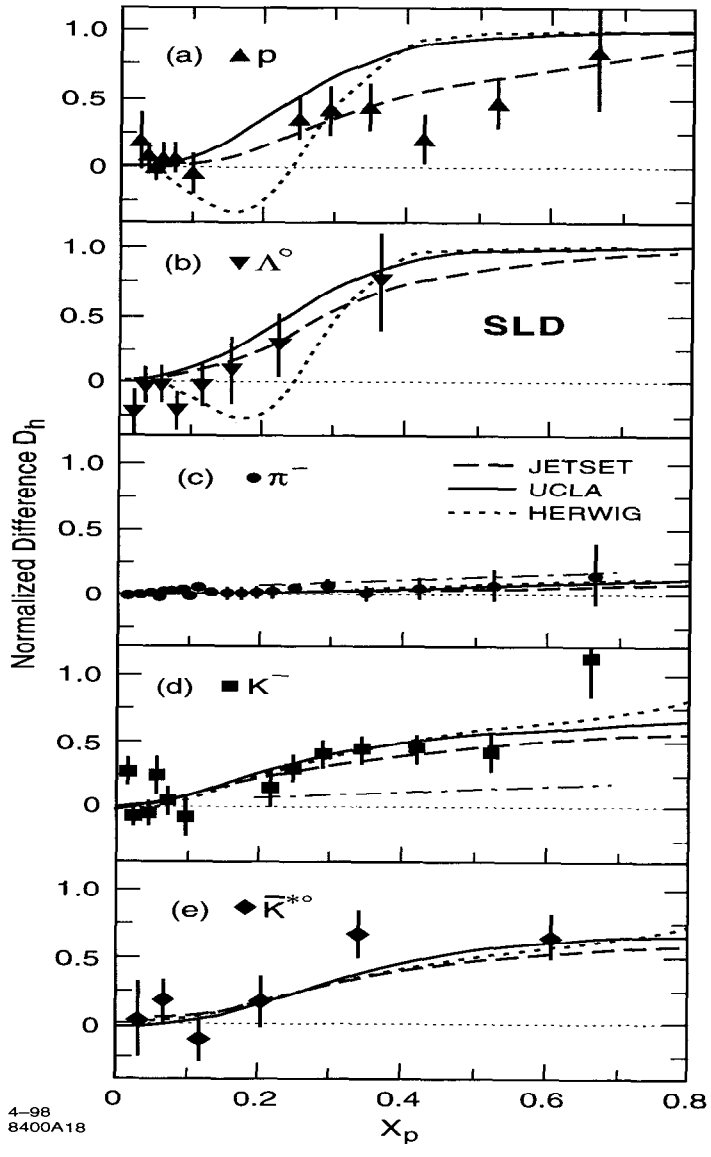

Fig. 4. Observation of leading particle effect.

high in this region and we cannot exclude that leading baryons are also produced at low x_p. Differences are also observed for both pseudoscalar and vector K-mesons, which indicate not only leading production of these two hadron species but also that leading strange mesons are produced more often from initial s quarks than from initial u or d quarks.

2.1.3 Hadron Correlations

We present a study of correlations in rapidity between pairs of identified pions, kaons and protons in hadronic Z^0 decays into light flavors. We observe excesses of opposite-charge over same-charge pairs for all pair types at low values of the absolute rapidity difference, $\mid y_1 - y_2 \mid$ in Fig. 5, indicating that there is a high degree of local conservation of baryon number, strangeness and electric charge in the fragmentation process.

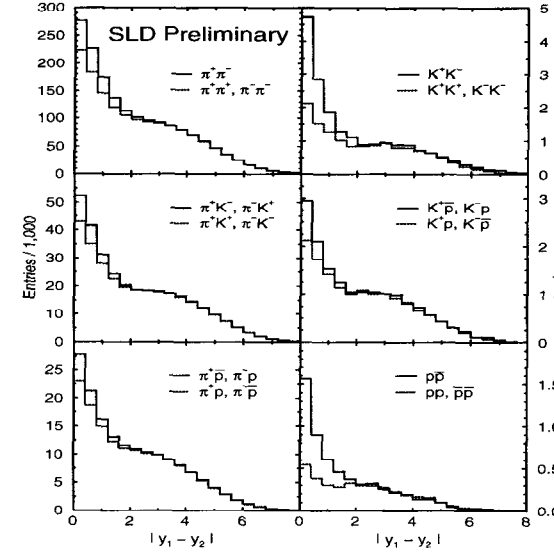

Fig. 5. Short range correlations due to local conservation of charge, strangeness and baryon number.

The range of these short-range correlations is found to be independent of momentum but to depend on the types of hadrons forming the pair. The predictions

of the JETSET fragmentation model are found to provide a qualitative description of the data, although they fail to describe the shapes of some of the correlations in detail. We observe a large excess of K^+K^- pairs over same-charge kaon pairs at large values of the absolute rapidity difference, and the effect is larger for higher momenta, as expected from leading kaon production in $s\bar{s}$ events. Considering only tracks with momentum greater than 9 GeV/c, we observe significant long-range correlations between opposite-charge $\pi\pi$, πK and Kp pairs, as well as KK pairs. The simulation provides a good description of the data in general, but predicts smaller long-range πK and Kp correlations than are observed, and predicts a small long-range πp correlation that is not observed.

The SLC electron beam polarization is used to tag the quark hemisphere in each event, allowing the first study of rapidities signed such that positive rapidity is along the quark rather than antiquark direction. Distributions of signed rapidities and of ordered differences between signed rapidities provide new insights into leading particle production and several new tests of fragmentation models.

We have studied distributions of rapidity signed so that positive rapidity corresponds to the quark (rather than antiquark) direction. Differences between signed rapidity distributions for positive and negative hadrons of all three types are observed, giving further evidence for leading production of charged pions, kaons, and protons. The distribution of the difference between the signed rapidities of p and $\bar{\text{p}}$ shows a large asymmetry at small values of the absolute rapidity difference indicating the ordering of baryons along the event axis. Ordered rapidity differences were also studied for other pair types, providing additional tests of fragmentation models.

2.2 Flavor Independence of α_s [6]

In this section we present a comparison of the strong coupling of the gluon to light ($q_l = u{+}d{+}s$), c, and b quarks, determined from multijet rates in flavor-tagged samples of hadronic Z^0 decays recorded at SLD between 1993 and 1995. Flavor separation among primary $q_l\bar{q}_l$, $c\bar{c}$, and $b\bar{b}$ final states was made on the basis of the topological vertex reconstruction described in section 1.1.

For the study of flavor-independence the jet structure of events was reconstructed in turn using six iterative clustering algorithms. We used the 'E', 'E0', 'P', and 'P0' variations of the JADE algorithm, as well as the 'Durham' ('D') and 'Geneva' ('G') algorithms.[7] In each case events were divided into two categories: those containing (i) two jets, and (ii) three or more jets. The fraction of the event sample in category (ii) was defined as the 3-jet rate R_3. This quantity is infrared- and collinear-safe and has been calculated to $\mathcal{O}(\alpha_s^2)$ in perturbative QCD.[7,8] For each algorithm we repeated the subsequent analysis successively across a range of values of the normalised jet-jet invariant-mass parameter y_c, $0.005 \leq y_c \leq 0.12$. In the final stage an 'optimal' y_c value was chosen for each algorithm so as to minimise the overall error on the analysis.

Each of the six jet-finding algorithms was applied to each tagged-event subsample j, ($j = 1,2,3$ for the uds, c, b subsamples) For each algorithm the 3-jet rate in each subsample was calculated. For the test of the flavor-independence of strong interactions it is convenient to consider the ratios (in which many systematic errors should cancel) of the 3-jet rates in heavy- and light-quark events, namely R_3^c/R_3^{uds} and R_3^b/R_3^{uds}. These were derived from the unfolded R_3^{uds}, R_3^c and R_3^b values.

The test of the flavor-independence of strong interactions can be expressed in terms of the ratios $\alpha_s^i/\alpha_s^{uds}$ ($i = c$ or b). Recalling that with our definition R_3 is the rate of production of 3 or more jets, $\alpha_s^i/\alpha_s^{uds}$ can be derived from the respective measured ratio R_3^i/R_3^{uds} using the next-to-leading-order perturbative QCD calculation:

$$\frac{R_3^i}{R_3^{uds}} = \frac{A^i\,\alpha_s^i + B^i(\alpha_s^i)^2 + O((\alpha_s^i)^3)}{A^{uds}\,\alpha_s^{uds} + B^{uds}(\alpha_s^{uds})^2 + O((\alpha_s^{uds})^3)} \tag{5}$$

where the coefficients A and B represent, respectively, the leading-order (LO) perturbative QCD coefficient for the 3-jet rate and the next-to-leading-order (NLO) coefficient for this rate.

For illustration, the measured ratios R_3^c/R_3^{uds} and R_3^b/R_3^{uds}, are shown in Fig. 6(a). R_3^b/R_3^{uds} lies above unity for the E, E0, P and P0 algorithms, and below unity for the D and G algorithms; note that all six data points are highly correlated with each other, so that the differences between algorithms are more significant than naively implied by the statistical errors displayed. For comparison, the corresponding QCD calculations of R_3^b/R_3^{uds} are also shown by the arrows in Fig. 6(a), under the *assumption* of a flavor-independent strong coupling with an input value of $\alpha_s(M_Z^2) = 0.118$, for $m_b(M_{Z^0}) = 3.0 \pm 0.5$ GeV/c^2. Under this assumption the calculations are in good agreement with the data, and the data clearly demonstrate the effects of the non-zero b-quark mass, which are larger than

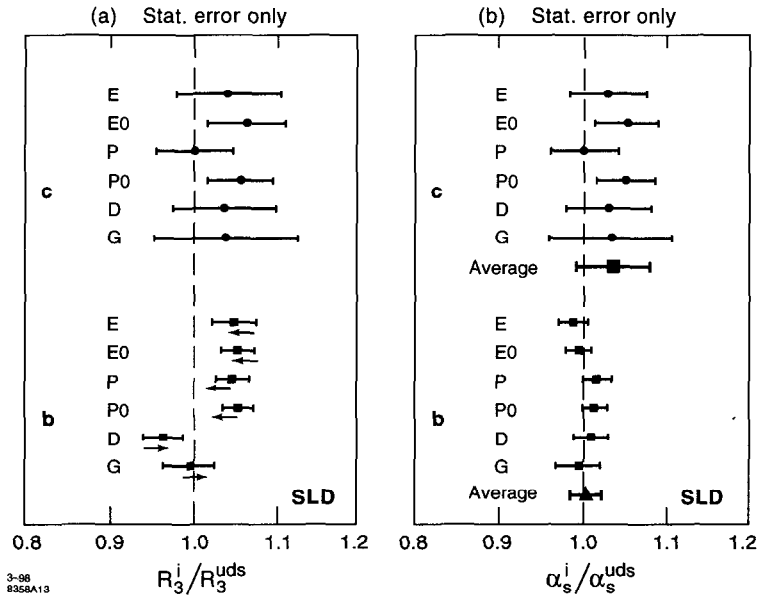

Fig. 6. Measured 3-jet rate ratios and corresponding α_s ratios for the 6 jet algorithms.

the statistical error. For the translation from R_3^b/R_3^{uds} to $\alpha_s^b/\alpha_s^{uds}$ we used a value of the running b-quark mass $m_b(M_{Z^0}) = 3.0$ GeV/c^2.

The $\alpha_s^c/\alpha_s^{uds}$ and $\alpha_s^b/\alpha_s^{uds}$ ratios are summarised in Fig. 6b. It can be seen that the ratios determined using the different jet algorithms are in good agreement with one another.

We obtained:

$$\alpha_s^c/\alpha_s^{uds} = 1.036 \pm 0.043(stat.)^{+0.041}_{-0.045}(syst.)^{+0.020}_{-0.018}(theory)$$
$$\alpha_s^b/\alpha_s^{uds} = 1.004 \pm 0.018(stat.)^{+0.026}_{-0.031}(syst.)^{+0.018}_{-0.029}(theory).$$

The theoretical uncertainties are only slightly smaller than the respective experimental systematic errors, and comprise roughly equal contributions from the hadronisation and translation uncertainties, as well as from the r.m.s. deviation over the six jet algorithms. We find that the strong coupling is independent of quark flavor within our sensitivity. Alternatively, under the assumption of the flavor independence of α_s, we derive $m_b(M_{Z^0}) = 3.23^{+1.02}_{-1.81}$ GeV/c^2.

2.3 Structure of $b\bar{b}g$ Events[9]

The observation of e^+e^- annihilation into final states containing three hadronic jets, and their interpretation in terms of the process $e^+e^- \to q\bar{q}g$, provided the first direct evidence for the existence of the gluon, the gauge boson of the theory of strong interactions, quantum chromodynamics (QCD). Following these initial observations, studies of the partition of energy among the three jets were performed at the DESY e^+e^- collider PETRA and SLAC e^+e^- storage ring PEP. Comparison of the data with leading-order QCD predictions, and with a model incorporating the radiation of spin-0 (scalar) gluons, provided qualitative evidence for the spin-1 (vector) nature of the gluon, which is a fundamental element of QCD.

In these studies the gluon jet was not explicitly tagged. Instead the jets were energy ordered and the lowest-energy jet was assumed typically to be the gluon jet. If the gluon jet could be tagged event-by-event more detailed studies of the structure of QCD could be performed. This is now possible at SLD using three-jet $b\bar{b}g$ events.

The chromomagnetic moment of the bottom quark is induced at the one-loop level in QCD and is of the order α_s/π. One can also write down an *ad hoc* Lagrangian[10] with a $b\bar{b}g$ coupling modified via anomalous chromoelectric and chromomagnetic moments:

$$\mathcal{L}^{b\bar{b}g} = g_s\bar{b}T_a\{\gamma_\mu + \frac{i\sigma_{\mu\nu}k^\nu}{2m_b}(\kappa - i\tilde{\kappa}\gamma_5)\}bG_a^\nu \qquad (6)$$

where g_s is the strong charge, T_a are the $SU(3)_c$ generators, m_b is the bottom quark mass, k is the outgoing gluon momentum, and κ and $\tilde{\kappa}$ parameterize the anomalous chromomagnetic and chromoelectric moments, respectively, which might arise from physics beyond the Standard Model. The effect of the former on three-jet observables has been calculated recently.[10] The latter is CP-violating, and in this analysis we have not attempted to discriminate between the b and $\bar{b}$ jets and are hence insensitive to non-zero values of $\tilde{\kappa}$ at leading order in $\tilde{\kappa}$. Non-zero values of κ would modify the gluon energy distribution in $b\bar{b}g$ events.

Charged tracks with large transverse impact parameters were used to tag $b\bar{b}$ events. Events with $N_{sig}^{evt} \geq 4$ were selected as $b\bar{b}$ events. This gave a $b\bar{b}$ sample with an estimated purity of 94.7%. Events were retained in which two jets were tagged as b or $\bar{b}$ by requiring them to have a number of significant tracks per jet $N_{sig}^{jet} \geq 2$. The remaining jet in each event was tagged as the gluon.

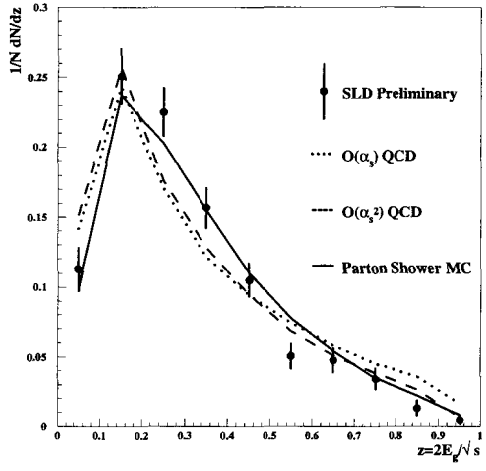

Fig. 7. Gluon energy spectrum. The Parton Shower (PS) MC agrees best with the data (e.g. around $z = 0.3$).

We studied the distribution of scaled gluon energy $z = 2E_{\rm gluon}/\sqrt{s}$. As the absolute value of κ is increased the gluon energy spectrum gets harder, producing an excess of gluon jets with high scaled energy. A difficulty arises in that the $O(\alpha_s)$ QCD calculation does not describe the data as well as the PS calculation, see Fig. 7, so that the higher-order QCD effects included in the PS prediction could be mimicked in the extended $O(\alpha_s)$ calculation by an artificially large anomalous moment κ.

A χ^2 minimisation fit was performed to the PS z distribution corrected with κ as the only free parameter. We find:

$$\kappa = -0.030^{+0.061}_{-0.062}(\text{stat.}) \tag{7}$$

We set 95% confidence-level upper limits of $-0.15 < \kappa < 0.09$.

2.4 B Hadron Energy Measurement[11]

The production of heavy hadrons (H) in e^+e^- annihilation provides a laboratory for the study of heavy-quark (Q) jet fragmentation. This is commonly characterised in terms of the observable $x_{E_H} \equiv 2E_H/\sqrt{s}$, where E_H is the energy of a B or D hadron containing a b or c quark, respectively, and $\sqrt{s}$ is the c.m. energy. In contrast to light-quark jet fragmentation, one expects[12] the distribution of x_{E_H}, $D(x_{E_H})$, to peak at an x_{E_H}-value significantly above 0. Since the hadronisation process is intrinsically non-perturbative $D(x_{E_H})$ cannot be calculated directly using perturbative Quantum Chromodynamics (QCD). However, the distribution of the closely-related variable $x_{E_Q} \equiv 2E_Q/\sqrt{s}$ can be calculated perturbatively and related, via model-dependent assumptions, to the observable quantity $D(x_{E_H})$; a number of such models of heavy quark fragmentation have been proposed.[13] Measurements of $D(x_{E_H})$ thus serve to constrain both perturbative QCD and the model predictions.

Here we describe the results of a new method for reconstructing the B-energy, inclusively, using only charged tracks from B decay vertices. An upper limit on the mass of the missing particles is found for each reconstructed B-decay vertex:

$$M_{0max}^2 = M_B^2 - 2M_B\sqrt{M_{ch}^2 + P_t^2} + M_{ch}^2. \tag{8}$$

where M_{ch} and P_t is the measured invariant mass and transverse momentum of the vertex tracks and M_B is the known B hadron mass. The true missing mass M_0 is hence bounded, $0 \leq M_0^2 \leq M_{0max}^2$, and the total B energy is well constrained when M_{0max} is small. In order to obtain an approximately x_B-independent selection efficiency we chose the *ad hoc* upper cut:

$$M_{0max}^2 < \left[1.1 + 6\frac{E_{beam} - E_B^{rec}}{1000} + 3.5e^{\frac{-(E_B^{rec}-5.5)}{3.5}}\right]^2$$

where the two terms that depend on the reconstructed energy E_B^{rec} increase the efficiency at lower B hadron energy. The overall efficiency for selecting B hadrons is 3.95% and the estimated B hadron purity is 99.5%.

We examined the B-energy resolution of this technique. The normalized difference between the true and reconstructed B hadron energies, $(x_B^{rec} - x_B^{true})/x_B^{true}$, for Monte Carlo events, was fitted by a double Gaussian, resulting in a core width of 10.4% and a tail width of 23.6%, with a core fraction of 83%.

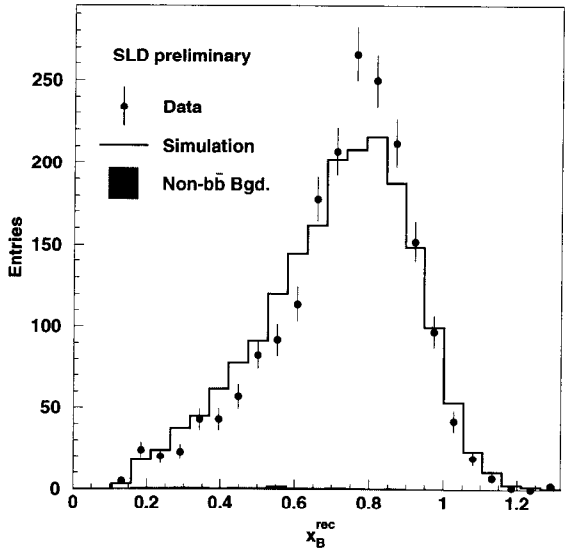

Fig. 8. Distribution of the reconstructed scaled B hadron energy for data (points) and Monte Carlo (histogram). The solid histogram shows the non-$b\bar{b}$ background.

A total of 1938 vertices in the data for 1996–97 satisfy all selection cuts. Figure 8 shows the distribution of the reconstructed scaled B hadron energy for data, $D^{data}(x_B^{rec})$, and for the Monte Carlo simulation, $D^{MC}(x_B^{rec})$. The distribution $D^{data}(x_B^{rec})$ was compared with various perturbative QCD, phenomenological and *ad hoc* model predictions. Each model was treated as an analytic functional form of $D(x_B^{rec})$. It is conventional to evaluate the mean of this distribution, $< x_B >$. For the three functions providing the best description of the data we took the average of the evaluated values of $< x_B >$ as the central result, and defined the unfolding uncertainty to be the r.m.s. deviation. Other systematic errors have not yet been included. We obtained:

$$< x_B > \; = 0.719 \pm 0.005(stat.) \pm 0.001(unfolding)$$

which is consistent with previous measurements. It was found that $< x_B >$ is relatively insensitive to the variety of allowed forms of the shape of the fragmentation function $D(x_B)$.

3 B Physics

3.1 B^+ and B^0 Lifetimes[14]

The spectator model predicts that the lifetime of a heavy hadron depends upon the properties of the constituent weakly decaying heavy quark Q and is independent of the remaining, or spectator, quarks in the hadron. This model fails for the charm hadron system for which the lifetime hierarchy $\tau_{D^+} \sim 2\tau_{D_s^+} \sim 2.5\tau_{D^0} \sim 5\tau_{\Lambda_c^+}$ is observed. Since corrections to the spectator model are predicted to scale with $1/m_Q^2$ the B meson lifetimes are expected to differ by less than 10% (Ref. 15). Hence a measurement of the B^+ and B^0 lifetimes provides a test of this prediction. In addition, the specific B meson lifetimes are needed to determine the element V_{cb} of the CKM matrix.

The analysis is performed using topologically reconstructed B decays in the 1993-98 data. The distance from the IP to the B decay location is the reconstructed decay length. Since the purity of the B charge reconstruction is lower for decays close to the IP, where tracks are more likely to be wrongly assigned, decay lengths are required to be > 1 mm. To avoid using the vertices of tracks originating from interactions with the detector material, the radial decay length is required to be < 24 mm for VXD2 (< 22 mm for VXD3), i.e. more than 1 mm inside the SLC beampipe.

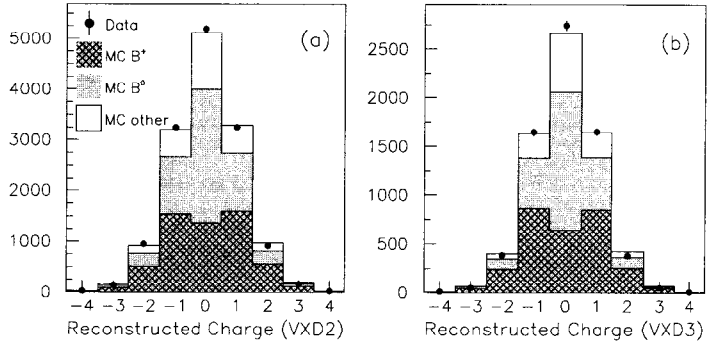

Fig. 9. Reconstructed vertex charge for data (points) and Monte Carlo (histogram) for (a) 1993-5 and (b) 1996.

Figure 9 shows a comparison of the reconstructed charge between data and

Monte Carlo for (a) VXD2 and (b) VXD3 (1996 only). At this stage the charged sample consists of 30028 vertices with vertex charge equal to $\pm$ 1,2 or 3, while the neutral sample consists of 19636 vertices with charge equal to 0 for the 1993-98 data. Monte Carlo studies indicate that for VXD3 the charged sample is 97.6% pure in B hadrons consisting of 55.1% B^+, 32.0% B^0, 8.6% B_s^0, and 4.3% B baryons. Similarly, the neutral sample is 98.2% pure in B hadrons consisting of 24.1% B^+, 54.1% B^0, 15.0% B_s^0 and 6.8% B baryons. The statistical precision of the measurement depends on the separation between the B^+ and B^0 in these samples.

The charge purity is a function of M_{P_T} and events are weighted accordingly. The initial state $b/\bar{b}$ tag (see section 3.5) is also used to enhance the charged sample purity by giving a higher (lower) weight to the B^+ hypothesis if the vertex charge agrees (disagrees) with the $b/\bar{b}$ tag.

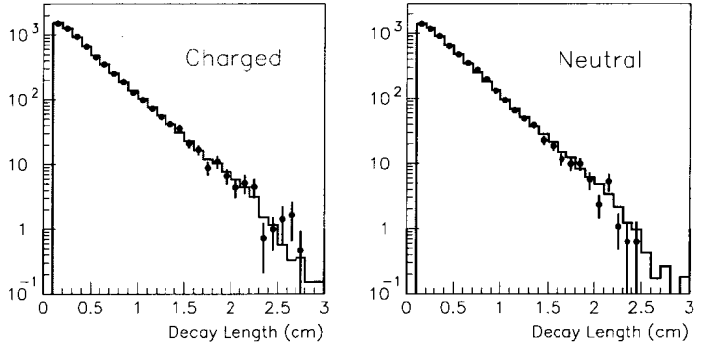

Fig. 10. Decay length distributions for 1997-8 data (points) and best fit Monte Carlo (histogram).

The B^+ and B^0 lifetimes are extracted from the decay length distributions of the B vertices in the charged and neutral samples using a binned χ^2 fit. These distributions are fitted simultaneously to determine the B^+ and B^0 lifetimes. Figure 10 shows the reconstructed decay length for data and best fit MC for the 1997-8 data and the charged and neutral samples.

The systematics are determined separately for the 1993-5, 1996 and 1997-8 measurements and then combined taking into account correlated uncertainties. The combined 1993-8 measurements yield the following result:

$$\begin{aligned} \tau_{B^+} &= 1.686 \pm 0.025(\text{stat}) \pm 0.042(\text{syst}) \text{ ps}, \\ \tau_{B^0} &= 1.589 \pm 0.026(\text{stat}) \pm 0.055(\text{syst}) \text{ ps}, \\ \frac{\tau_{B^+}}{\tau_{B^0}} &= 1.061 \pm^{0.031}_{0.029} (\text{stat}) \pm 0.027(\text{syst}). \end{aligned}$$

These results are consistent with the expectation that the B^+ lifetime is up to 10% greater than that of the B^0 and have the best statistical accuracy of the current measurements.

3.2 Search for Charmless B Decays

Four exclusive charmless hadronic channels listed in the first column of table 1 have been studied. The decays involve either $\rho^0 \to \pi^+\pi^-$ or $K^{*0} \to K^+\pi^-$ producing a 3-prong final state. Hence the initial selection requires a 3-prong vertex (reconstructed from all track combinations) with a total charge of ± 1. A Fischer discriminant function is constructed from eight kinematic variables, each parametrized for signal and background. The variables used include vertex mass and energy, ρ^0 or K^{*0} mass, and the centre-of-mass helicity angle. The resulting Fischer discriminant distribution for signal and background is shown in Fig. 11.

	Theory	CLEO	DELPHI	ALEPH	SLD	SLD ϵ
$B^+ \to \rho^0\pi^+$	0.4 – 1.4	5.8	16	3.2	8.2	0.50
$B^+ \to \rho^0 K^+$	0.01 – 0.06	1.4	12		9.2	0.45
$B^+ \to K^{*0}\pi^+$	0.6 – 0.9	3.9	39		7.9	0.52
$B^+ \to K^{*0}K^+$					9.0	0.46

Table 1. Theoretical prediction and experimental 90% C.L. upper limits (BR$\times 10^{-5}$). SLD signal efficiency, ϵ, is shown in last column.

The cut in the Fischer discriminant is chosen such as to minimize the expected upper limit using Monte Carlo. The ability to compete with other experiments is due to the high vertexing efficiency at SLD. The signal efficiencies are around 50% as listed to the right in table 1. No candidate signal events are seen in the 1993-98 SLD data from which the SLD limits shown in the table are derived.

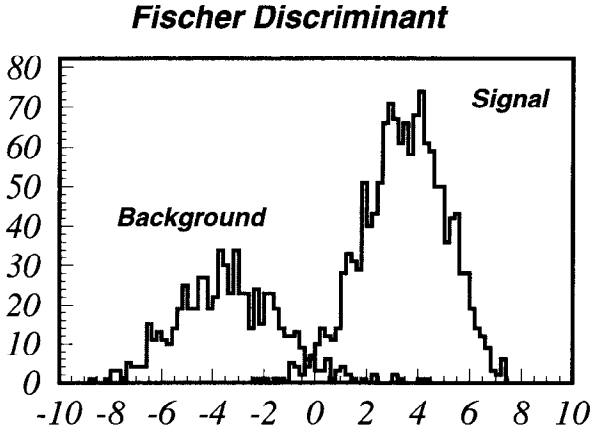

Fig. 11. Fischer discriminant based on eight kinematic variables.

3.3 Search for $b \to sg$ [16]

The low measured B semileptonic decay branching ratio (BR) and charm production deficit in B decays compared to theoretical expectations has been a persistent puzzle in B physics. This has left room for B decays from possible mechanisms beyond the Standard Model with BR as large as 10%. In the Standard Model, flavor changing neutral current decays of the type $b \to s\, g^{(*)}$ (including $b \to sg$ and $b \to sq\bar{q}$) have a total branching ratio of $\approx$ 1% (Ref. 17). One hypothesized scenario is that the $b \to sg$ decay is enhanced to a BR of 10% by new physics.[18] Such a scenario is consistent with all existing experimental constraints, including the measured BR($b \to s\gamma$), and would nicely explain the above puzzles.

The signal for $b \to sg$ is a high momentum kaon from the B decay. In experiments where the B's have significant boost, such as SLD at the Z^0 pole, it is rather difficult to derive the momentum of the B decay kaon in the B rest frame due to the uncertainty in the B boost. We circumvent this difficulty by using the kaon momentum transverse to the B flight direction (p_t). A key factor making this analysis viable at SLD is the excellent particle identification capability of the SLD Cerenkov Ring Imaging Detector to allow efficient use of $K^\pm$ production. The analysis is performed using the 300,000 Z^0 decays collected during 1993-1997.

For the evaluation of analysis sensitivity to the $b \to sg$ process, we used the JETSET inspired model[19] with a specific set of parameter choices as a bench mark test. Figure 12 shows the projected p_t spectrum for $K^\pm$ produced in standard $b \to c$ decays and in $b \to sg$ decays for BR($b \to sg$) = 10% and 15% from this model. For $p_t > 1.8$, the ratio of $b \to sg$ to $b \to c$ approaches unity for $BR(b \to sg) \approx 10\%$ so that a $b \to sg$ signal should appear as a clear excess in this region.

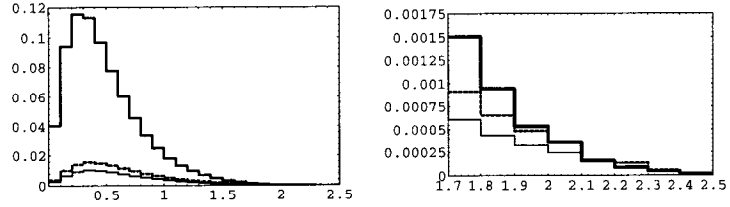

Fig. 12. $K^\pm$ p_t spectra (GeV/c) for standard $b \to c$ (heavy line) and for $b \to sg$ with BR=10% (light line) and BR=15% (medium line). The first plot shows the whole spectrum and the second shows the high-p_t region.

Charm lifetimes are long enough that tracks arising from their cascade decays will often be inconsistent with the B-decay vertex. In contrast, all tracks associated with a $b \to sg$ decay should fit to a single vertex. The data is therefore split into two samples: "1-Vertex" where all tracks identified as coming from the B decay cascade fit to a single vertex, and "2-Vertex" where they do not; $b \to sg$ events should show up primarily in the 1-Vertex sample.

$K^\pm$,$p_t > 1.8$	1 vertex	All
	# events	# events
Data	37.0	93.0
$b \to c$ MC	29.0	78.2
Difference	8.0 ± 6.1	14.8 ± 9.6
BR($b \to sg$)=10%	24.0	33.3

Table 2. Comparison of number of high p_t $K^\pm$ expected and observed in the 1- and 2-vertex samples.

Figure 13 shows the p_t spectra for identified $K^\pm$ in the 1- and 2-vertex samples. The Monte Carlo was normalized to the data by the number of tagged

b-hemispheres. Table 2 gives the total number of $K^{\pm}$ with $p_t > 1.8$ Gev in both samples. Small excesses are seen in both the 1- and 2-vertex samples indicating that no significant signal for $b \to sg$ is observed.

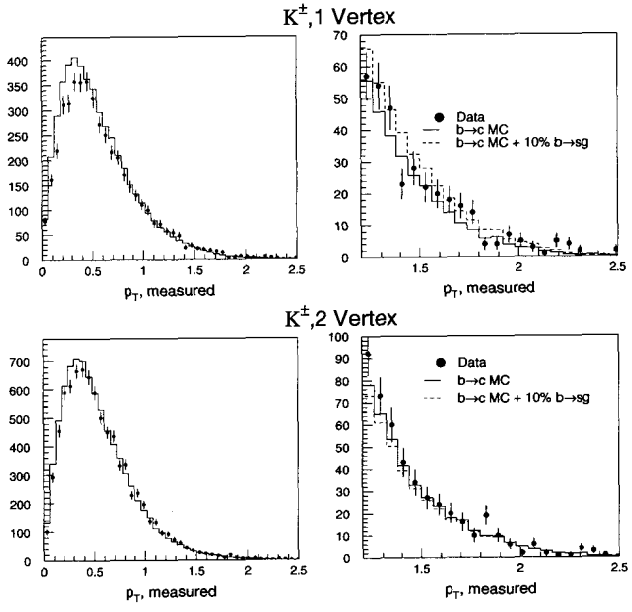

Fig. 13. Comparison of data to Monte Carlo p_t spectrum of identified $K^{\pm}$ in the 1- and 2- vertex samples. The solid line shows the Monte Carlo predicted spectrum of standard $b \to c$ decays. The dashed line shows the predicted spectrum for BR($b \to sg$)=10%.

The observation of kaons with $p_t > 1.8$ GeV/c in the 1-vertex sample yields a result of $8.0 \pm 6.1 \pm 5.9$ events over an expected background of 29 events. After correcting for $K^{\pm}$ identification efficiency, this yields a high-p_t production excess of $(5.0 \pm 3.8 \pm 3.6) \times 10^{-4}$ per B decay. This corresponds to a statistical precision of $\pm 2.5\%$ on the $b \to sg$ branching ratio for a particular set of choices of $b \to sg$ model parameters.

We have demonstrated that this measurement technique already has interesting statistical precision to test the hypothesis of a largely enhanced $b \to sg$ branching ratio at the 10% level, even with a rather small input data sample. Data taken in 1998 will be added in the near future, and this will approximately double the data statistics.

3.4 Double-Charm B Decays

The excellent vertex resolution at SLD also allows a measurement of the process $B \to D\overline{D}X$ resulting from the quark transition $b \to c\bar{c}s$. The tracks from the topologically reconstructed B decays are required to have a 1-vertex fit probability of $< 5\%$ and are separated into a secondary and tertiary vertex. The task is then to estimate whether these two vertices are the B and D vertices of a $B \to$ 1-charm decay or the $\overline{D}$ and D vertices of a $B \to$ 2-charm decay. Two techniques are employed. The first counts the number of identified kaons in each vertex. For $B \to D\overline{D}X$ decays a greater proportion of events will have a kaon in the secondary (D decay) vertex compared with $B \to$ 1-charm decays (where the secondary is the B decay). By comparison with Monte Carlo the fraction of double charm decays in the data $f_{D\overline{D}}$ is extracted, see table 3.

	CLEO	DELPHI	ALEPH	SLD Kaon	SLD D charge
$f_{D\overline{D}}$	18 ± 4	17 ± 4	$25 \pm 4 \pm 4$	$18.8 \pm 2.5 \pm 5.9$	19.5 ± 4.5

Table 3. Measurements of the double charm branching fraction $B \to D\overline{D}X$ (%).

The second technique utilizes the beam polarization and the jet charge to tag the $b/\bar{b}$ flavor of the B. The correlation between this tag and the charge of the tertiary vertex is again sensitive to $f_{D\overline{D}}$. This second measurement gives a result consistent with the kaon analysis, as can be seen in table 3. Current work is aimed at combining these techniques and reducing the systematic error.

3.5 B_s Mixing[20]

Transitions between B^0 and $\overline{B^0}$ mesons take place via second order weak interactions. In the Standard Model, a measurement of the oscillation frequency Δm_d for B^0_d–$\overline{B^0_d}$ mixing determines, in principle, the value of the Cabibbo-Kobayashi-Maskawa matrix element $|V_{td}|$, which is parameterized in terms of the Wolfenstein parameters ρ and (the CP-violating phase) η, both of which are currently poorly

constrained. However, theoretical uncertainties in calculating hadronic matrix elements are large ($\sim$ 25% [Ref. 21]), and thus, limit the current usefulness of precise Δm_d measurements. These uncertainties are significantly reduced ($\sim$ 6–10%) for the ratio between Δm_d and Δm_s. Thus, combining measurements of the oscillation frequency of both B_d^0–$\overline{B_d^0}$ and B_s^0–$\overline{B_s^0}$ mixing translates into a measurement of the ratio $|V_{td}|/|V_{ts}|$ and provides a stronger constraint on the parameters ρ and η.

Experimentally, a measurement of the time dependence of B^0–$\overline{B^0}$ mixing requires three ingredients: (i) the B decay proper time has to be reconstructed, (ii) the B flavor at production (initial state $t = 0$) needs to be determined, as well as (iii) the B flavor at decay (final state $t = t_{\rm decay}$). At SLD two methods using the same initial state flavor tag but using different techniques to reconstruct the B decay and tag its final state flavor have been studied. The data consists of 250,000 hadronic Z^0 decays collected with the upgrade vertex detector (VXD3) during 1996-98.

The probability that a meson created as a B_s^0 ($\overline{B_s^0}$) will decay as a $\overline{B_s^0}$ (B_s^0) after proper time t can be written as

$$P_m(t) = \frac{\Gamma}{2}\, e^{-\Gamma t}\, [1 - \cos(\Delta m_s\, t)] \ . \tag{9}$$

where Δm_s is the mass difference between the mass eigenstates, Γ is the average decay width of the two states and P_m denotes the probability to 'mix'. The effects of CP violation are assumed to be small and are neglected.

The probability for a decay to be tagged as mixed is expressed taking into account the fraction of each b-hadron type (B^+, B_d^0, B_s^0, and b-baryon), as well as their lifetimes and mistag probabilities, and $udsc$ background (this gives $\mathcal{P}_m(t, \Delta m_s)$). Detector and vertex selection effects are then introduced by convoluting the above probability functions with a proper time resolution function $\mathcal{R}(T, t)$ and a time-dependent efficiency function $\varepsilon(t)$:

$$P_m(T, \Delta m_s) = \int_0^\infty \mathcal{P}_m(t, \Delta m_s)\ \mathcal{R}(T, t)\ \varepsilon(t)\ dt \ , \tag{10}$$

where t is the "true" time and T is the reconstructed time. Again, a similar expression applies to the unmixed probability P_u. The resolution function is parameterized by the sum of two Gaussians with the core fraction set to 60%. The proper time resolution is a function of proper time and also depends on the measured boost $\gamma\beta = p_B/m_B$, its resolution $\sigma_{\gamma\beta}$ and on the estimate of the decay length resolution σ_L.

A tag of the initial state flavor is provided by the large polarized forward-backward asymmetry for $Z^0 \to b\,\bar{b}$ decays:

$$\tilde{A}_{FB} = 2A_b\ \frac{A_e - P_e}{1 - A_e P_e}\ \frac{\cos\theta_T}{1 + \cos^2\theta_T} \ , \tag{11}$$

where $A_b = 0.94$ and $A_e = 0.150$ (Standard Model values), P_e is the electron beam longitudinal polarization, and θ_T is the angle between the thrust axis and the electron beam direction (the thrust axis is signed such that it points in the same hemisphere as the reconstructed vertex). Thus, left- (right-) polarized electrons tag b ($\bar{b}$) quarks in the forward hemisphere, and $\bar{b}$ (b) quarks in the backward hemisphere.

The tag is enhanced by the addition of other flavor-sensitive quantities derived from tracks in the opposite hemisphere, utilizing: a jet charge technique, the total track charge and charge dipole (see below) of the opposite hemisphere vertex (if found) and the charge of identified kaons or leptons in the opposite hemisphere. The various tags are combined to form an overall initial state tag b-quark probability. The average correct tag probability is 0.80 with full efficiency.

3.5.1 Lepton+D Analysis

The lepton+"D" analysis aims at reconstructing the B and D vertex topologies of semileptonic B decays. It proceeds by first selecting event hemispheres containing an identified lepton (e or μ) with $|\cos\theta| < 0.7$. Then, a D vertex candidate is reconstructed using a similar topological technique as that described earlier. Several cuts are added to clean up the D vertex candidate and reduce the contamination from cascade ($b \to c \to l$) charm semileptonic decays. The final state B^0 or $\overline{B^0}$ flavor is tagged by the sign of the lepton charge.

The B decay vertex is reconstructed by intersecting the lepton and D trajectories. To enhance the fraction of B_s^0 decays, the sum of lepton + D vertex track charges is required to be $Q = 0$. This enhances the B_s^0 fraction to 15.3% of selected b hadrons in the $Z^0 \to b\bar{b}$ MC (the B_s^0 production fraction in the $Z^0 \to b\bar{b}$ MC is 11.5%). A sample of 1492 decays is thus obtained in the 1996-98 data.

Reconstruction of the b-hadron boost uses both tracking and calorimeter information. The overall performance of the decay length and boost measurements

for B_s^0 decays proceeding via the direct $(b \to l)$ transition is shown in Fig. 14.

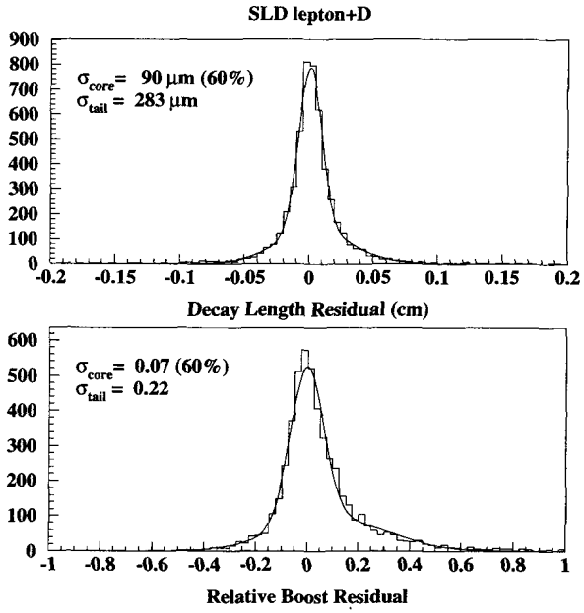

Fig. 14. Distributions of the decay length and relative boost residuals for B_s^0 $(b \to l)$ decays in the simulation.

For each decay, the resolution σ_L is computed from the vertex fit and IP position measurement errors. The relative boost residual $\sigma_{\gamma\beta}/\gamma\beta$ is parameterized as a function of the lepton + D vertex total track energy, with parameters extracted from the MC simulation. Similarly, the efficiency $\varepsilon(t)$ is parameterized using the MC simulation. All parameterizations are performed separately for each b-hadron type.

3.5.2 Vertex Charge Dipole Analysis

The Charge Dipole analysis aims at reconstructing the B and D vertex topologies in inclusive decays, and tags the B_s^0 or $\overline{B_s^0}$ decay flavor based on the charge difference between the B and D vertices. This analysis technique is unique to SLD. Hemispheres containing an inclusive topological vertex with $M_{P_T} > 2$ GeV/c^2 are selected and the total vertex track charge Q is required to be 0. To select decays with non-negligible separation between the B and D decay points, the probability for fitting all tracks to a single vertex is required to be less than 1%. The tracks are then rearranged into various two-vertex combinations and the combination with the lowest overall χ^2 is selected. The vertex that is closer to the IP is labelled "B" and that further away is labelled "D."

A "Charge Dipole" is defined as $\delta Q \equiv D_{BD} \times SIGN(Q_D - Q_B)$, where D_{BD} is the distance between the two vertices and Q_B (Q_D) is the charge of the B (D) vertex. Positive (negative) values of δQ tag $\overline{B_s^0}$ (B_s^0) decays and the correct tag probability increases with increasing $|\delta Q|$.

For all data and MC events, hemispheres already containing a vertex selected by the lepton+D analysis are removed such that the two analyses are statistically uncorrelated. A total of 5719 decays remain in the dipole sample. Figure 15 displays the distribution of charge dipole δQ for the data sample and also indicates the separation between b hadrons containing b or $\bar{b}$ quarks in the MC.

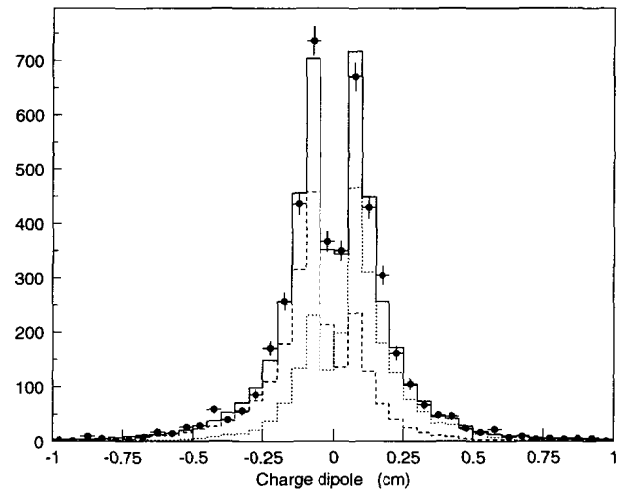

Fig. 15. Distribution of the vertex charge dipole for data (points) and Monte Carlo (solid histogram). Also shown are the contributions from b hadrons containing a b quark (dotted histogram) or a $\bar{b}$ quark (dashed histogram).

3.5.3 Amplitude Fit

The study of the time dependence of B_s^0–$\overline{B_s^0}$ mixing is carried out using the amplitude method described in Ref. 22. Instead of fitting for Δm_s directly, the analysis is performed at fixed values of Δm_s and a likelihood fit to the amplitude A of the oscillation is performed, i.e. in the expression for the mixed and unmixed probabilities, one replaces $[1 \pm \cos(\Delta m_s t)]$ with $[1 \pm A\cos(\Delta m_s t)]$. This method is similar to Fourier transform analysis and has the advantage of facilitating the combination of results from different analysis techniques and different experiments.

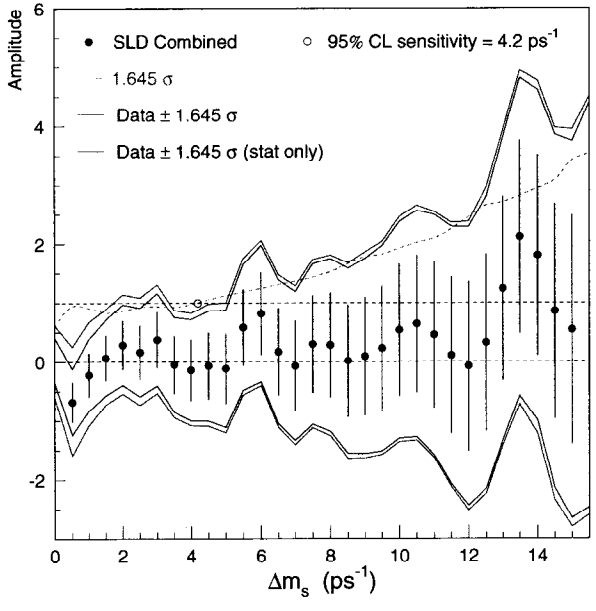

Fig. 16. Measured amplitude as a function of Δm_s the combined analyses.

The lepton+D and Charge Dipole analyses are combined taking into account correlated systematic errors. Figure 16 shows the measured amplitude as a function of Δm_s for the combination. The measured values are consistent with $A = 0$ for the whole range of Δm_s up to 15 ps^{-1} and no evidence is found for a preferred value of the mixing frequency. The following ranges of B_s^0–$\overline{B_s^0}$ oscillation frequencies are excluded at 95% C.L.: $\Delta m_s < 1.7$ ps^{-1} and $3.3 < \Delta m_s < 5.0$ ps^{-1}, i.e., the condition $A + 1.645\,\sigma_A < 1$ is satisfied for those values. The combined sensitivity to set a 95% C.L. lower limit is found to be at a Δm_s value of 4.2 ps^{-1}.

It is worth noting that the overall sensitivity is expected to improve rapidly as the rest of the 1998 data and more analysis techniques are added.

4 Summary and Conclusions

The unique features of SLD and SLC have helped produce world best or competitive results in B physics and QCD. Most of the QCD results are yet to be updated using the 1996-98 data with the upgraded vertex detector. It is the flavor tagging abilities at SLD that have resulted in competitive studies of the flavor independence of α_s, the structure of $b\bar{b}g$ events and a measurement of the B hadron energy. By utilizing particle identification and the e^- beam polarisation new tests of fragmentation models have been performed.

The precise vertexing has been most beneficial in the studies of B physics. The worlds best measurement of the lifetime ratio of the B^+ and B^0 has been made and unique analysis of charmless and double-charm B decays has been possible. A competitive limit for B_s oscillations already exists and will improve with updated tagging techniques. In particular, with more data from the proposed SLD run extension a strong constraint on the CKM unitarity triangle will be made, complementary to the results from the B-factories.

References

[1] K. Abe *et al.*, *Design and Performance of the SLD Vertex Detector, a 307 Mpixel Tracking System*, Nucl. Inst. Methods A **400**, 287 (1997).

[2] K. Abe *et al.*, Phys. Rev. D **53**, 1023 (1996).

[3] D. J. Jackson, *A Topological Vertex Reconstruction Algorithm for Hadronic Jets*, Nucl. Inst. Methods A **388**, 247 (1997).

[4] K. Abe *et al.*, *A Measurement of R_b using a Vertex Mass Tag.*, Phys. Rev. Lett. **80**, 660 (1998).

[5] K. Abe *et al.*, *Production of π^+, K^+, K^0, K^{*0}, ϕ, p and Λ^0 in Hadronic Z^0 decays*, Phys. Rev. D **59**, 052001 (1999).

K. Abe *et al.*, *A Study of Correlations between Identified Charged Hadrons in Hadronic Z^0 decays*, SLAC-PUB-7824; June 1998.

[6] K. Abe *et al.*, *An Improved Test of the Flavor Independence of Strong Interactions*, Phys. Rev. D **59**, 012002 (1999).

[7] S. Bethke *et al.*, Nucl. Phys. B **370** (1992) 310;
erratum: Nucl. Phys. B **523**, 681 (1998).

[8] Z. Kunszt *et al.*, CERN 89–08 Vol. I, 373 (1989).

[9] K. Abe *et al.*, *A Preliminary Study of the Structure of $b\bar{b}g$ Events using Z^0 decays*, SLAC-PUB-7822; June 1998.

[10] T. Rizzo, Phys. Rev. D **50** (1994) 4478.

[11] K. Abe *et al.*, *A Preliminary Improved Measurement of the B Hadron Energy Distribution in Z^0 decays*, SLAC-PUB-7826; June 1998.

[12] See, for example, J.D. Bjorken, Phys. Rev. D **17**, 171 (1978).

[13] M.G. Bowler, Z. Phys. C **11**, 169 (1981); C. Peterson, D. Schlatter, I. Schmitt and P.M. Zerwas, Phys. Rev.D **27**, 105 (1983); B. Andersson, G. Gustafson, G. Ingelman, T. Sjöstrand, Phys. Rep. **97**, 32 (1983).

[14] K. Abe *et al.*, *Measurement of the B^+ and B^0 Lifetimes using Topological Vertexing at SLD*, SLAC-PUB-7868; July 1998.

[15] See, for example, I. I. Bigi *et al.*, in *B Decays*, edited by S. Stone (World Scientific, New York, 1994), p. 132.

[16] K. Abe *et al.*, *Inclusive Search for $b \to sg$*, SLAC-PUB-7896; July 1998.

[17] A. Lenz, U. Nierste, and G. Ostermaier, Phys. Rev. D **59**, 034008 (1999); A. Lenz, U. Nierste, and G. Ostermaier, Phys. Rev. D **56**, 7228 (1997).

[18] A.L. Kagan, Phys. Rev. D **51**, 6196 (1995); M. Ciuchini, E. Gabrielli and G. F. Giudice, Phys. Lett. B **388**, 353 (1996); B.G. Grzadkowski and W.-S. Hou, Phys. Lett. B **272**, 383 (1991).

[19] A. Kagan and J. Rathsman, `hep-ph/9701300`.

[20] K. Abe *et al.*, "Time Dependent B_s^0–$\overline{B_s^0}$ Mixing Using Inclusive and Semileptonic B Decays at SLD," SLAC-PUB-7885; July 1998.

[21] P. Paganini, F. Parodi, P. Roudeau, and A. Stocchi, Phys. Scripta **58**, 556 (1998) and `hep-ph/9802289`.

[22] H.-G. Moser and A. Roussarie, Nucl. Inst. Methods A **384**, 491 (1997).